[Downloaded from www.aece.ro on Thursday, July 03, 2025 at 19:18:59 (UTC) by 172.69.6.6. Redistribution subject to AECE license or copyright.]

Data-Driven Predictive Control of a Pneumatic Ankle Foot Orthosis

Osman ULKIR[1], Gazi AKGUN[2], Ahad NASAB[3], Erkan KAPLANOGLU[4]
[1]*Department of Electronics and Automation, Mus Alparslan University , 492109, Turkey*
[2]*Department of Mechatronics Engineering, Marmara University , 34210, Turkey*
[3,4]*Department of EMT, Mechatronics, University of Tennessee at Chattanooga, 37403, USA*
erkan-kaplanoglu@utc.edu

***Abstract*—We present the design and control of a pneumatic ankle-foot orthosis (P-AFO) device powered via bi-directional pneumatic rotary actuator and a pneumatic artificial muscle for rehabilitation assistance and treatment of neuromuscular disorders. The rotary actuator and the pneumatic muscle assist with dorsiflexion and plantar flexion, respectively. The prototype is also equipped with simple sensor system for gait pattern analysis. The P-AFO has the capability of 20 degrees dorsiflexion from the plantar flexion and 12 degrees dorsiflexion from the neutral position of an ankle joint. The data-driven predictive control (DDPC) algorithm has been designed for P-AFO to follow desired gait cycle trajectories while rectifying the nonlinearity and uncertainties of the pneumatic actuators. The design of DDPC is realized from the subspace identification matrices acquired by the input-output values obtained as a result of an open-loop operation. The control structure is completely data-based without certain use of a model in the control implementation. In order to control the developed P-AFO prototype device, the suggested controller was implemented in a real-time operating system. Experimental studies are performed to compare the proposed controller with a three-term controller (PID) in trajectory tracking of the P-AFO.**

***Index Terms*—rehabilitation assistance, ankle-foot orthosis, subspace identification, PID, data-driven predictive control.**

I. INTRODUCTION

The facility for an orthosis device to enforce an assistive torque (e.g., dorsiflexion and plantar flexion) at the ankle joint and to control position and motion of the ankle could be important to the rehabilitation process with ankle-foot orthosis [1]. Users could get utility from an ankle-foot orthosis for rehabilitation assistance for ankle disorders in accidents and for treatment of the neuromuscular disorders such as polio, stroke, trauma, cerebral palsy, and multiple sclerosis. Because of these problems, foot-slap, drop-foot and toe-drag gait disorders occur in the ankle joint [2-5]. The main reason of neuromuscular impairment is the weakness of the dorsiflexor and the plantar flexor. Impaired patients are motivated subjects for these devices as a result of the high number of lower extremity injuries seen in last decades [6].

There are various treatments for ankle-foot disabilities such as surgical, orthotic, or therapeutic. Functional electrical stimulation (FES) is one of the active e methods of gait treatment [7.8]. These devices use surface electrodes for stimulating the peroneal nerve to assist the ankle dorsiflexor to provide functionality throughout the swing phase of the gait cycle. During this stimulation, the ankle may be tensed behind natural angle, which helps the ankle foot complex maintain toe clearance during the swing phase. The size and duration of the stimulation can be adjusted to change gait pattern. FES devices provide the actuation and assistance that passive ankle-foot orthosis provides, but the devices don't help the plantar flexion during gait [9].

Among these treatment types, orthotic treatment is the most common implementation. This method can be used for drop-foot and foot-slap prevention [10]. An ankle-foot orthosis (AFO) device is defined as a type of exoskeleton which surrounds the ankle and foot. AFO devices could be divided into three categories which are passive, semi active, and active. Passive AFO devices are not comprised of active controllers, onboard electronic or electrical components, and a power supply. Passive AFOs were not designed to assist people in workout and train weak muscles [11]. Additionally, disadvantage of long-term use is neural conformations that gradually decrease muscle activity in time. Thus, passive AFOs generally put more pressure on physical therapy to correct these unwanted long-term effects. Semi active AFOs are able to change flexibility of the ankle joint using computer control [12]. A semi-active, passive AFO that has been configured for motion control lacks the ability to assist a user that has plantar flexor deficiencies. As a result, there are few orthotic strategies for the loss of plantar flexion.

Active orthotic devices have been developed to direct the limitations of passive and semi-active AFOs by supplying power to the ankle joint for torque assistive and motion control. Active AFOs include actuators, power sources, sensors, and control systems. These active devices vary according to the actuation principle and/or control strategy.

Actuation principles can be categorized into two main groups: active AFOs powered by means of series elastic actuators (SEAs) and active AFOs powered by means of pneumatic artificial muscles (PAMs). The majority of these orthosis devices using for assisting the ankle joint only in a sagittal plane throughout walking. Their goal is to show the effect of an orthosis device on the human ankle kinematics when assistance is provided to both dorsiflexion and plantarflexion movements or only to the gait cycle"s the plantarflexion phase. The SEAs consist of motor-actuated ball-screw mechanism in series with a helical spring [13-14]. The motor is designed to provide torque assistance via a driven screw. The screw changes the height of the spring in order to achieve rotary compliance. While the elastic actuators are comfortable enough for daily use, AFOs are

Digital Object Identifier 10.4316/AECE.2021.01007

1582-7445 © 2021 AECE

[Downloaded from www.aece.ro on Thursday, July 03, 2025 at 19:18:59 (UTC) by 172.69.6.6. Redistribution subject to AECE license or copyright.]

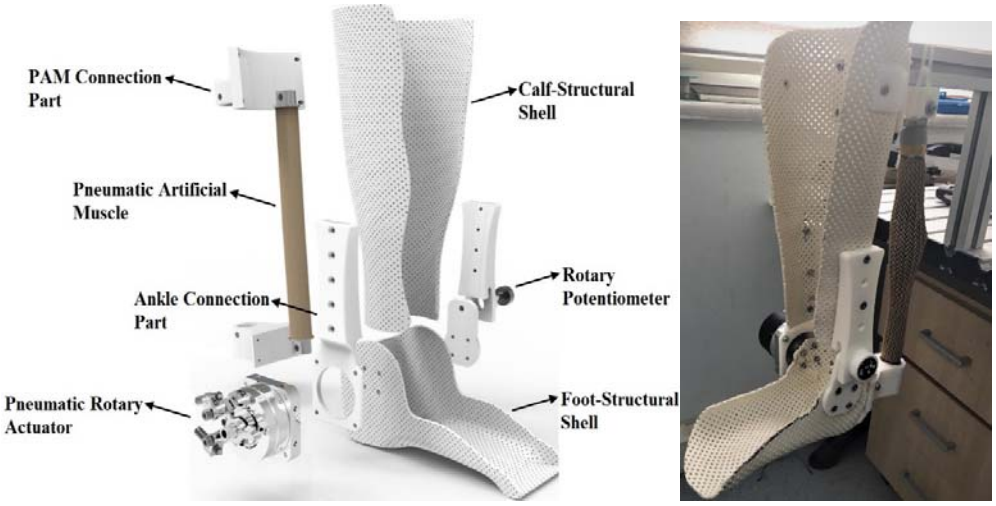

Figure 1. Main design of the P-AFO device. (a) Design concept; (b) Actual prototype

bulky and ill-suited for daily wear due to the various power transmission components within. They also do not provide the high torque assistance required for the walking cycle. The PAMs consist of an expandable internal bladder surrounded by a braided shell. When air pressure is applied, it expands in a balloon like manner and shortens in the axial direction. Thus, PAMs generate large contraction forces which rely on the strength of the applied pressure. PAMs are desirable for active AFO devices because they are light-weight, capable of high forces, and inherently compliant. PAMs have been used for research or clinical rehabilitation treatments that help patients recover from pathological disorders or injuries [15, 16]. Artificial muscles are not suitable for daily wear, but they produce high torque assistance compared to SEAs and provide three plane (sagittal, transvers and frontal) support. Electric motors and hydraulic systems have also been applied as both series and direct-drive elements for active AFOs [17-20].

Control schemes developed for active AFOs depend on the fact that the gait is essentially a cyclical motion. Pre-programmed patterns, that may be set as information about the present kinematic/kinetic state and the function of the stride time, have been proposed to mimic the ankle behavior. Various methods have been used in the controller design problem of active AFOs, including trajectory tracking control, torque control, and variable impedance control. [21-24]. Control algorithms such as PID, impedance, and adaptive are used to solve this controller problem [25-27]. Many of these control algorithms are model-based. The fact that the active AFOs developed will be used on different people increases the importance of the controller. The success of the controller will facilitate the adaptation of the device to the user and for this reason, it is important to develop the controller to be independent of the model. Therefore, data-driven predictive control (DDPC) algorithm is proposed as the control method in this study. The most important reason for choosing the DDPC is to estimate the model of the P-AFO by making a subspace identification. DDPC chosen as a result of this purpose is subspace based, and it can converge the model of the P-AFO to the real model along the horizon determined by the input-output values obtained as a result of an open-loop operation [28-30]. Although model-based control ensures a higher positioning precision for active AFOs compared to data-driven control, its design process requires that the system be modelled and that there be an adequate knowledge of control theory, making it difficult for designers.

To the best of our knowledge, this is the first study to design an active AFO device with a hybrid actuator structure and control it with data-driven predictive control algorithm.

In this article, we present a novel active orthotic device powered by bidirectional pneumatic rotary actuator and pneumatic artificial muscle for use in treatment of neuromuscular disorders and in rehabilitation assistance. The major benefits of fluid power in this device are the force to volume ratios of the actuators and high force to weight alongside having the ability to operate a joint without the need for a more traditional power transfer method. It also uses flexible hoses to transport the pressurized fluid to the actuator, and these hoses can be placed in locations along the body where it would be impossible for a traditional motor to reach. Subspace identification method was used for model estimation of P-AFO. DDPC algorithm chosen as a result of this purpose is subspace based. DDPC consists of the subspace based predictor and the cost function of the model predictive control (MPC) algorithm. For performance comparison of the DDPC and the PID in trajectory tracking of the P-AFO, experimental studies were performed. The real-time experimental results demonstrate that the P-AFO device satisfies the design requirements, controllability of ankle joint angles and suggested control algorithm is better than the PID controller. The rest of the article is organized as follows. Section II describes the design and fabrication of the prototype. Section III presents the control strategy and the designed DDPC algorithm. Section IV shows experimental studies. Section V shows the result of experimental studies. We conclude with a general conclusion of the study.

II. P-AFO DESIGN

The P-AFO consists of subsystems that house structure, sensing, actuation, and power (Fig. 1). We used portable

[Downloaded from www.aece.ro on Thursday, July 03, 2025 at 19:18:59 (UTC) by 172.69.6.6. Redistribution subject to AECE license or copyright.]

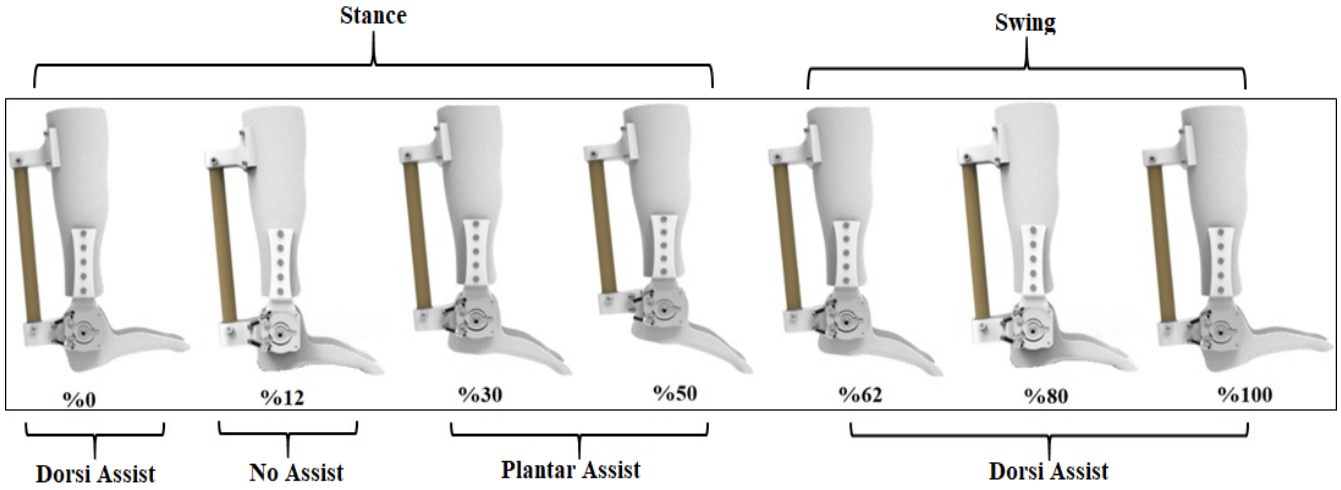

Figure 2. Cycle was divided into multiple phases defined by functional gait task

battery powered air compressor (SMC,800kPa) and pressure regulator (SMC, MCQ 134) to power pneumatic artificial muscle (FESTO,DMSP-20-120N-RM-CM)and bidirectional rotary actuator (FESTO,DSM-12-270-P-FW-A-B) at the ankle joint. Compressed air is used safely near the human body in a number of widespread applications. We used the equipment within the specifications manual of the manufacturer to provide user safety during operation.

The calf and ankle-foot components were custom-fabricated from orfit thermoplastic material over a model of a leg and were the structural elements of the system. This material offers high comfort for patients and is very easy to use. A large diversity in width and thickness allows one to treat a wide range of pathologies and to accommodate different orthotic designs. The connection parts used for pneumatic artificial muscle, pneumatic rotary actuator and rotary potentiometer are manufactured using PLA filament in a 3D printer.

Pneumatic artificial muscle (PAM) is attached behind the distal shank part of P-AFO. PAM is responsible for plantar flexion motion on sagittal plane. As PAM contracts, its artificial tendon pulls the anchoring points on the foot brace resulting in plantar flexion of the foot. From the end of the mid stance through toe off, P-AFO have provided plantar flexion assist to prevent drop-foot. High forces can be obtained depending on the applied air pressure value using PAM. PAMs are widely used in rehabilitation robots to generate high force and motions with soft-flexible structures. Pneumatic rotary actuator (PRA) is mounted at the lateral shank part of P-AFO. PRA is responsible for dorsiflexion motion on sagittal plane. As the PRA is actuated, it pulls the anchoring points on the ankle resulting in dorsiflexion of the foot. During heel strike, the P-AFO provides dorsiflexion assist to prevent foot-slap. During swing, torque assistance is provided to prevent drop-foot. The foot part was allowed to rotate through the 90° range of motion (ROM) ability of the PRA. PRA can produce 20 Nm assistive torque according to the applied air pressure without the need for any transmission.

The direction of the motion could be switched from dorsiflexion to plantar flexion with proportional directional control valves (FESTO, MPYE-5-1/8-HF-010 B). The switching control of the proportional valve was chosen according to the events during the gait cycle. We assigned the event limits for these states using a rotary potentiometer (10 kΩ (np22) endless rotation) placed in the ankle joint.

In the P-AFO, the ankle ROM is between -20° and 12° for sagittal plane. The total weight of the developed P-AFO prototype is 2.5 kg excluding power supply and air compressor.

III. P-AFO CONTROL

The importance of the controller increases for the fact that AFOs will be used on different people. Because the success of the controller will facilitate the adaptation of the device to the user, it is important to develop the controller independently of the model. Therefore, data-driven predictive control algorithm was proposed as control method to estimate the model of the P-AFO by making subspace identification. The data-driven predictive control algorithm was designed with the use of subspace identification method. DDPC chosen as a result of this purpose is subspace based, and it can converge the model of the P-AFO to the real model along the horizon determined by the input-output values obtained as a result of an open-loop operation. With the model obtained as a result of the identification, a control rule has been written for the predictive control cost function.

In order to provide the appropriate assistance during gait, we controlled the position of P-AFO. Position of both the plantar flexion and dorsiflexion motions were adjusted by the proportional directional control valve. The control system comprised of a potentiometer at the ankle joint. This sensor helps detect the movement of foot.

Timing of the P-AFO position was adjusted by distinct functional gait requirements (Fig. 2). During the loading response (%0-%12), the P-AFO controlled dorsiflexion angle prevent foot slap. In midstance (%12-%30), the P-AFO ensured no assistance and permitted of free ROM at the ankle joint. The wearer was stabilized by the structure of the device during midstance. From the beginning of terminal stance through pre-swing (%30-%62), plantar flexion angle was controlled to assist propulsion. During swing (%62-%100), dorsiflexion angle was controlled to prevent foot drop by maintaining toe clearance.

It is very important to choose the control algorithm for the P-AFO to perform successful position tracking during the walking cycle. Unlike industrial applications, it is a

[Downloaded from www.aece.ro on Thursday, July 03, 2025 at 19:18:59 (UTC) by 172.69.6.6. Redistribution subject to AECE license or copyright.]

desirable variable for the patient's treatment process to proceed in a healthy way, in which the actuator is connected with successful follow-up performance in Biomechatronics applications. The fact that the developed P-AFO will operate with a multi-user operation, requires that the patient quickly adapts to the foot. As a result of a simple and fast experiment, a control algorithm that optimally adapts to the patient's foot is required for fast and effective treatment. In addition, the robotic system, which is designed as a multi-user, is required to work with the best fit for every user.

It creates a unique model when the foot is physically attached to the robot due to the difference of the healing process of each user or the unique mechanical characteristic of the foot. Original models need to be estimated to achieve the targeted fit.

In this study, subspace identification method was used for model estimation. The data-driven predictive control (DDPC) algorithm chosen as a result of this purpose is subspace based, and it can converge the model of the system to the real model along the horizon determined by the input-output values obtained as a result of an open-loop operation. In addition, the fact that the control algorithm works by looking at past input and output values during a specified horizon ensures that any improvement or abnormal conditions that will occur during the continuous treatment process are added to the control rule and the treatment process progresses in a synchronous manner.

The novelty of the DDPC algorithm over other control techniques is that the system does not have the traditional, explicit parametric definition, such as the state-space model in the development of the controller or transfer function. Instead, it uses the subspace-based parameter estimation equation to predict future output values of the system. Therefore, the predictive control algorithm is also called 'data-driven' or 'model-free' predictive control [31-33]. In addition, subspace based parameter estimation equation coefficients are obtained directly from offline input-output (I/O) data by performing a single QR decomposition from a specific Hankel data matrix. Once the appropriate parameter estimation coefficients are obtained, a model can be applied to the predictive control algorithm and consequently results in the application of the DDPC algorithm. The rule based on past data is able to respond quickly by following all the actions along the horizon. The key features of the developed controller are as follows:

- The controller theory is designed using I/O data with on-line and off-line mechanisms and the cost function of the model predictive control (MPC).
- DDPC does not need a system model to develop the concept of control. The system model is created by estimation methods.
- The data is taken as knowledge without mathematical models or implicit and explicit information.
- DDPC algorithm can be easily applied to multi-input and multi-output systems.

In this section, the mathematical modelling of DDPC algorithm used in the control of P-AFO will be explained. In order to create the proposed control algorithm, subspace-based parameter estimation and model predictive control algorithm will be explained, respectively.

A. Subspace Identification Method

This subsection provides the background on the subspace identification matrices from the open loop data. These matrices will be used in the following section to design a data-driven predictive controller. The subspace method accepts the state space model as the system model structure.

The basic principle of subspace parameter estimation is based on the fact that the state, the input and output vectors, and the state space parameters (A, B, C, D) can be easily estimated by least mean square regression methods. We can set up the routine in the first order differential equation form using the input and output signals and the state vector, such as the state-space model shown in Equation 1.

$$\begin{aligned} x_{k+1} &= Ax_k + Bu_k + Ke_k \\ y_k &= Cx_k + Du_k + e_k \end{aligned} \tag{1}$$

where, $u_k \in \mathbb{R}^m$, $y_k \in \mathbb{R}^l$ and $x_k \in \mathbb{R}^m$ are the input variables, the output variables and the state vector variables of the system, respectively, and $e_k \in \mathbb{R}^l$ is the white noise disturbance. The system matrices $A \in \mathbb{R}^{nxn}, B \in \mathbb{R}^{nxm}$, $'p'$ and $K \in \mathbb{R}^{lxl}$ are the state, input, output, feed-through and Kalman filter gain matrices, respectively.

The measurements of the inputs, u_k, and the outputs, $y_k \left(k \in \{1,2,\ldots,N\}\right)$, are assumed to be accessible for system identification and the input Hankel matrices for u_k, represented as U_p and U_f. The indexes $'f'$ and $'p'$ represent the 'future' and 'past' matrices of the variables. Similarly, Hankel matrices for y_k, are represented as Y_f and Y_p. The system past and future state sequences are defined as below:

$$x_p = \begin{bmatrix} x_1 & x_2 & \ldots & x_{N-2M+1} \end{bmatrix} \tag{2}$$

$$x_f = \begin{bmatrix} x_{M+1} & x_{M+2} & \ldots & x_{N-M+1} \end{bmatrix} \tag{3}$$

In the subspace identification method, these Hankel matrices are made to be rectangular. Thus, the undesired effects of noise on the identification system are minimized. This condition can be achieved by having a large data set, indicated by the variable *N*. Moreover, *M* represents the order of the predictor equation [34]. For successful identification, the order *M* must be bigger than or at least equal to the real system order *n* as demonstrated in the size of the state matrix A.

The subspace prediction expression of the outputs can be derived by recursive substitution of Equation 1 [35, 36].

$$Y_f = \Gamma_M X_f + H_M^d U_f \tag{4}$$

$$Y_p = \Gamma_M X_p + H_M^d U_p \tag{5}$$

$$X_f = A^M X_p + \Delta_M^d U_p \tag{6}$$

$\Gamma_M \in \mathbb{R}^{Mlxn}$ can be described as the extended observability matrix, $\Delta_M^d \in \mathbb{R}^{nxMm}$ as reversed prolonged

[Downloaded from www.aece.ro on Thursday, July 03, 2025 at 19:18:59 (UTC) by 172.69.6.6. Redistribution subject to AECE license or copyright.]

deterministic controllability matrix, and $H_M^d \in \mathbb{R}^{nxMl}$ as the triangular Toeplitz matrix. The optimal prediction of Y_f can be written as follows:

$$\hat{Y}_f = L_w W_p + L_u U_f \tag{7}$$

where, W_p indicates the past input-output data matrix as $W_p = \begin{bmatrix} Y_p & U_p \end{bmatrix}^T$, L_w and L_u are the subspace matrices corresponding to the past input-output data and future input data, respectively. The following least squares problem is solved to calculate the subspace matrices L_w and L_u from Hankel matrices.

$$\min_{L_w, L_u} \left\| Y_f - \begin{bmatrix} L_w & L_u \end{bmatrix} \begin{bmatrix} W_p \\ U_f \end{bmatrix} \right\|_F^2 \tag{8}$$

This problem can be solved from shifting the orthogonal projection of the row space Y_f into the row space of the matrix $W_p = \begin{bmatrix} Y_p & U_p \end{bmatrix}^T$. This can be defined by Equation (9) shown below:

$$\hat{Y}_f = Y_f / \begin{bmatrix} W_p \\ U_f \end{bmatrix} \tag{9}$$

where, / indicates the orthogonal projection. The solution for Equation (9) can be done by performing QR-decomposition as follows:

$$\begin{bmatrix} W_p \\ U_f \\ Y_f \end{bmatrix} = R^T Q^T \begin{bmatrix} R_{11} & 0 & 0 \\ R_{21} & R_{22} & 0 \\ R_{31} & R_{32} & R_{33} \end{bmatrix} \begin{bmatrix} Q_1 \\ Q_2 \\ Q_3 \end{bmatrix} \tag{10}$$

where, R is a low triangular matrix and Q is an orthogonal matrix.

$$L = \begin{bmatrix} R_{31} & R_{32} \end{bmatrix} \begin{bmatrix} R_{11} & 0 \\ R_{21} & R_{22} \end{bmatrix}^{\dagger} = \begin{bmatrix} L_w & L_u \end{bmatrix} \tag{11}$$

where, † denotes the Moore-Penrose pseudoinverse and $L_w \in \mathbb{R}^{MlxM(m+1)}, L_u \in \mathbb{R}^{MlxMm}$.

B. Data-Driven Predictive Control

The Data-Driven Predictive Control (DDPC) consists of the subspace based predictor defined in section A and the cost function of the model predictive control (MPC) algorithm. In this section, using the calculated estimation equation coefficients L_w and L_u, the controller gains $K_{\Delta w_p}$ and K_e are calculated. Control theory is written using these coefficients, the past input-output, and the future output data. The controller performs optimization at every step. The first set of control signals calculated at each step is applied to the P-AFO.

The minimization of a cost function is the realization of the MPC problem. The cost function in MPC with the typical form of is given as shown below:

$$J = \sum_{k=1}^{N_p} \left(\hat{y}_{t+k} - r_{t+k} \right)^T W_Q \left(\hat{y}_{t+k} - r_{t+k} \right) + \sum_{k=1}^{N_c} \Delta u_{t+k-1}^T W_R \Delta u_{t+k-1} \tag{12}$$

where, W_Q and W_R are the weight matrices, r_t is the reference signal at present t, N_p, and N_c are the prediction and control horizon, respectively. These horizon parameters are defined as being equal to *f*. Using Equation (7) and the reference signal, the cost function can be rewritten as:

$$\begin{aligned} J = & \left(L_w \Delta w_p + L_u^{N_c} \Delta u_{N_c} + y_t - r_{t+1} \right)^T w_Q x \\ & \left(L_w \Delta w_p + L_u^{N_c} \Delta u_{N_c} + y_t - r_{t+1} \right) + \Delta u_{N_c}^T \end{aligned} \tag{13}$$

When the cost function is solved, the control rule can be written as:

$$\begin{aligned} \Delta u_f = & -\left(\left(L_u^{N_c} \right)^T W_Q \left(L_u^{N_c} \right) + W_R \right)^{-1} x \left(L_u^{N_c} \right)^T W_Q \\ & \left(L_w \Delta w_p + \left(y_t - r_{t+1} \right) \right) = -K_{\Delta w_p, N_c} \Delta w_p - K_{e, N_c} \left(y_t - r_{t+1} \right) \end{aligned} \tag{14}$$

$K_{\Delta w_p, N_c}$ and $-K_{e, N_c}$ are the weight of the past data and the tracking error, respectively. At each time instance, only the first element of Δu_f is used to calculate the control input. Therefore the control input u_t is determined as follows:

$$u_t = u_{t-1} + \Delta u_t \tag{15}$$

The proposed DDPC algorithm was performed on the P-AFO. The control system architecture is shown in Fig. 3. In Fig. 3, M and N are the length of data and $y_d(k+1), y(k+1), u(k-M)$ are the desired output and the real output and input, respectively. All input-output data are stored in a database to use in the control method. This data is generated off-line using MATLAB and transferred to PAM and PRA through serial communication between the computer and the microcontroller.

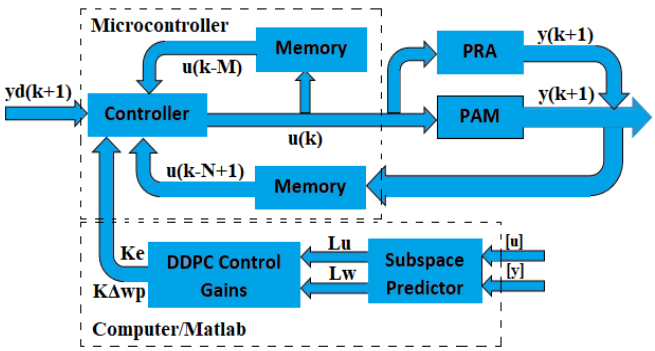

Figure 3. Control system architecture

The collected input-output data are used for subspace identification in MATLAB. After determining the appropriate parameter estimation coefficients (L_w, L_u) with subspace identification, the model became applicable to the

[Downloaded from www.aece.ro on Thursday, July 03, 2025 at 19:18:59 (UTC) by 172.69.6.6. Redistribution subject to AECE license or copyright.]

model predictive control algorithm. As a result, DDPC algorithm becomes implementable. The values $K_{\Delta w_p}$, K_e calculated in MATLAB are sent to the microcontroller via serial communication. The control algorithm is then executed on microcontroller with those values and actual I/O data through control horizon.

DDPC and PID controllers were compared. The trajectory was determined based on functional gait cycle as shown in Fig. 2. This trajectory includes dorsiflexion and plantar flexion movements in the sagittal plane. The dorsiflexion angle includes [0-10] angles, and the plantar flexion angles includes [0; -15].

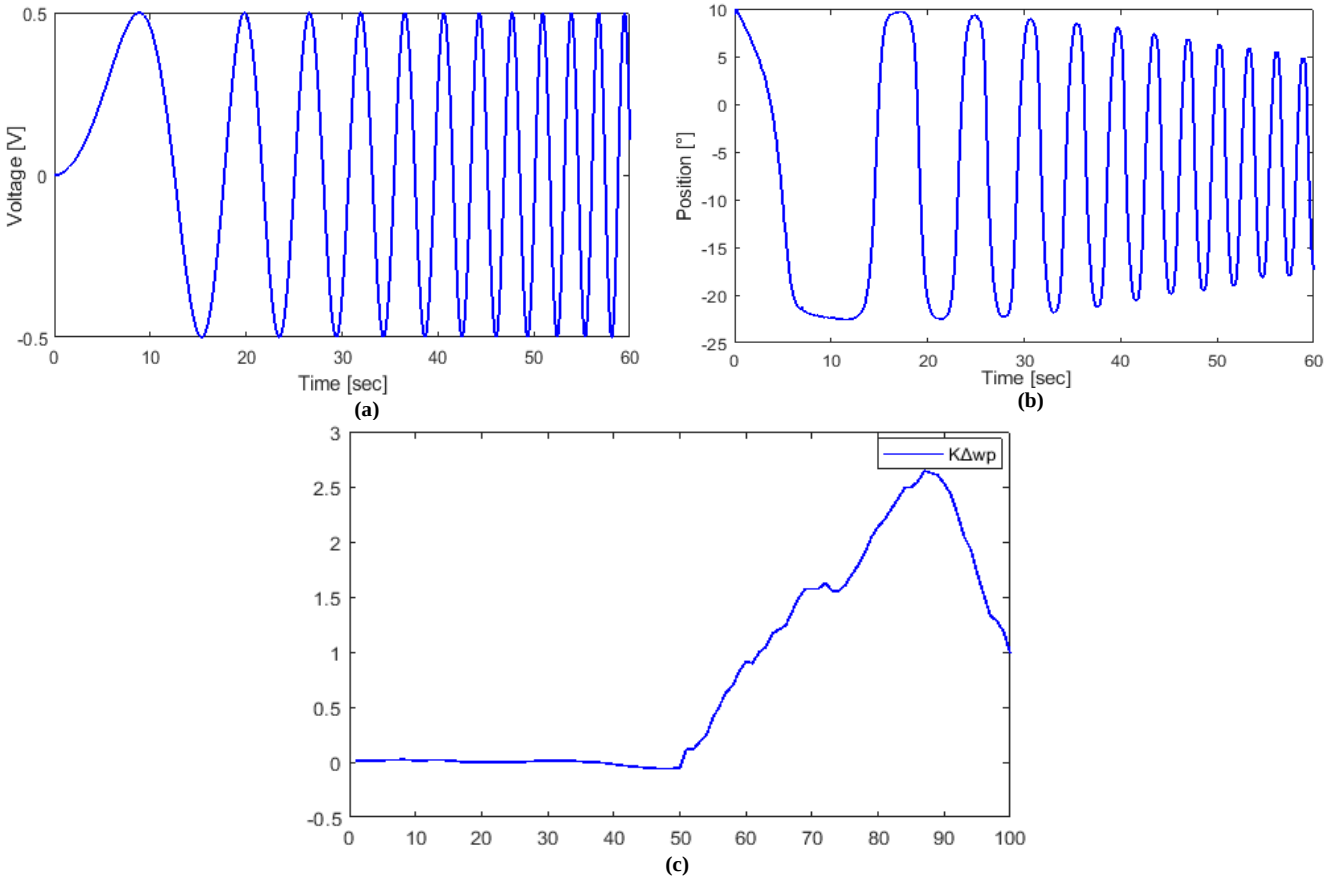

Figure 4. Subspace identification data for P-AFO and DDPC control gains.
(a) Sine input signal with scanning frequency; (b) Output signal measured from P-AFO; (c) DDPC control gains, $K_{\Delta w_p}$, K_e

IV. Experiments

The data-driven predictive controller was applied to the P-AFO for position control, based on the theory given in Section III. Experimental studies were implemented to show the performance of the P-AFO device, to characterize the designed actuator, as well as compare the performance of the proposed DDPC and the PID controller. The coefficients of the PID controller are chosen as *Kp=8*, *Ki=3*, and *Kd=2* respectively. Experimental studies consist of step response, multi-step response, stride frequency, and trajectory tracking. The P-AFO prototype was fixed to a rigid stationary table to hang in the air as shown in Fig. 1 (b). Experimental studies were carried out on the P-AFO without being worn by a user.

On the first study, step and multi-step response studies were implemented for comparison of time reaction of the controllers.. Three step inputs of -10°, -15°, -20° and the multi-step trajectory within the range of [3°; 8°; 12°] were given to the P-AFO as reference positions. Responses of the DDPC and PID controllers to the position step and multi-step inputs were analyzed.

As a second study, trajectory tracking performances of the

Finally, stride frequency study was implemented to characterize the tracking performance of the data-driven predictive controller with changing walking speeds. The experiment was implemented on the P-AFO to track a sine signal trajectory with amplitude of 10° and at various frequencies of 0.4 Hz, 0.6 Hz, and 0.8 Hz.

The P-AFO position was directly measured using rotary potentiometer which is attached in the ankle joint. The control algorithm was implemented by MATLAB on a PC with a sampling time of 20 ms. This sampling time was selected to accomplish an optimal control performance and to be suitable for the bandwidth of the used proportional directional control valve.

The working ranges of the P-AFO device were adjusted as below:

$$u \in [0;10](V)\, y \in [12;-20](^\circ)\, P \in [0;6](bar)$$

Here, u, y, and P are the driving voltage range of the proportional valve, the position, and pressure of PAM, respectively.

To design the predictive controller, the input/output data collected from the open-loop experiment are necessary to define the subspace matrices with subspace identification

[Downloaded from www.aece.ro on Thursday, July 03, 2025 at 19:18:59 (UTC) by 172.69.6.6. Redistribution subject to AECE license or copyright.]

method. Many different experimental studies have been performed for subspace identification. By changing the input signals applied to the P-AFO in the experiments, we attempt to obtain the best identification signal. In these experiments, a sine signal with a single frequency value, a sine signal produced in two and three different frequencies, and a sine signal with scanning frequency were applied, respectively.

When the model obtained after applying these input signals was compared to the state space model of P-AFO, the average success was higher in the scanning frequency signal which is a form of signal that starts from the low frequency component and continues to increase in the specified range. It has been determined that the input signal, which includes components in many different frequency ranges with constant amplitude, will provide better recognition of the system's characteristics. The experimental studies were implemented with a sine signal with scanning frequency of magnitude 0.5 for the inputs.

The subspace parameter estimation matrices, $L_u(100x100), L_w(100x100)$ are decided using subspace identification, $i=100(row)$ and $j=100(column)$ in the Hankel matrices. The range of the Hankel matrices was set as $N_c=10, f=50$ and $p=10$, while the weighting matrices are selected as $W_Q=100$,and $W_R=1000$. The input signal applied to P-AFO for subspace identification, the output signal measured from the system and the DDPC control gains, $K_{\Delta w_p}, K_e=0.0235$ are shown in Fig. 4. These gains calculated using Equation (14). The important coefficients from calculating the control gains are N_c, f, p, W_Q and W_R. The optimal coefficients are calculated as above and real-time control of the P-AFO is carried out by applying the control gains to the DDPC control rule determined in Equation (15).

V. Experimental Results

In the first experiment, step and multi-step input response experiments were implemented to compare the behavior over time of both controllers. The recorded responses of the DDPC and PID controllers to three position step inputs are shown in Fig. 5. Red lines symbolize the position step inputs of -10°, -15°, -20°. These reference position values represent plantar flexion angle values during gait cycle.

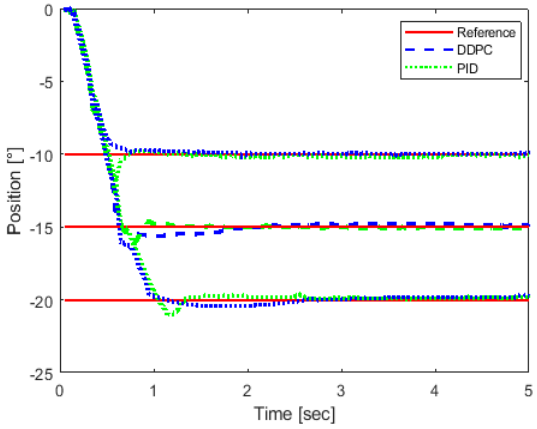

Figure 5. Position step input responses of the DDPC and PID controller

The working time for each reference is determined as 5 seconds. The responses of the DDPC are symbolized using blue lines, while the green lines represent the PID controller step input response. Performance indices of the PID controller and DDPC are showed in Table I. Percentage overshoot values, rise time, settling times, and RMS error measurements are submitted.

TABLE I. Performance Indexes of the Step Response Experiment

	-10°		-15°		-20°	
	DDPC	PID	DDPC	PID	DDPC	PID
Percentage overshoot (%)	5.21	19.45	4.17	13.7	2.53	9.72
Rise time (sec)	0.43	0.44	0.57	0.65	0.87	0.94
Settling time (sec)	1.05	1.28	1.50	1.95	2.05	2.39
RMS Error (°)	2.21	3.85	3.60	5.47	4.42	9.85

As shown in Fig. 5, the experimental data indicates that the DDPC has a more accurate response to the position step inputs than the PID controller. The percentage overshoot performance of the DDPC is in the preferable level to the PID controller as shown in Table 1. If rise times are considered, it seems that the two controllers perform closely. When the comparison is made in terms of settling times, it can be realized that the DDPC outperforms PID controller. However, the output reached setpoint in a short time in both controllers. RMS error performances of the controllers are close to each other, but the DDPC has performed better. Settling times of the active AFO actuators have been shown to be within 0.5 s and 1.5 s [37, 38]. Therefore, the designed actuator is sufficient for the design requirement of low response time.

The recorded responses of the DDPC and PID controllers to three position multi-step inputs are shown in Fig. 6. Red lines symbolize the position step inputs of 3°, 8°, and 12°. These reference position values represent dorsiflexion angle values during gait cycle.

The working time for each reference is determined as 10 seconds. The responses of the DDPC are symbolized using blue lines, while the green lines represent the PID controller step input response. Performance indexes of the DDPC and PID controller are dedicated in Table II. Percentage overshoot, rise time, settling times, and RMS error measurements are presented.

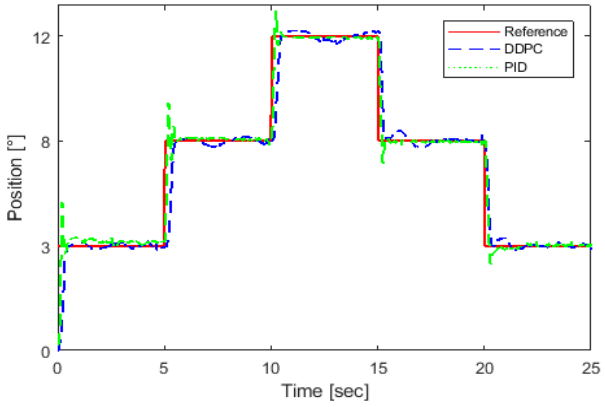

Figure 6. Position multi-step input responses of the DDPC and PID controller

[Downloaded from www.aece.ro on Thursday, July 03, 2025 at 19:18:59 (UTC) by 172.69.6.6. Redistribution subject to AECE license or copyright.]

When the experimental results are examined, it is seen that the position of P-AFO can be controlled at the desired level in the multi-step responses with DDPC as shown in Fig. 6. Considering the overshoot values that are shown in Table II, the DDPC shows more than twice performance the PID controller. Among the reference trajectory changes, the PID controller responded with high overshoot against short rise time, while DDPC responded with a low overshoot against a slightly longer rise time.

TABLE II. PERFORMANCE INDEXES OF THE MULTI-STEP RESPONSE EXPERIMENT

	3°		8°		12°	
	DDPC	PID	DDPC	PID	DDPC	PID
Percentage overshoot (%)	9.15	34.8	7.54	32.5	6.83	28.54
Rise time (sec)	0.40	0.35	0.61	0.51	0.79	0.72
Settling time (sec)	1.85	2.95	2.57	3.92	3.15	4.71
RMS Error (°)	1.95	2.98	2.40	3.95	3.12	4.87

If settling times are considered, it can be understood that the DDPC performs slightly better than the PID controller. RMS error performances of the controllers are close to each other, but the DDPC has performed better. As a result, the DDPC generated a good transient response and steady-state performance compared to the PID controller.

In the second experiment, trajectory tracking performances of the DDPC and PID were compared. This trajectory includes dorsiflexion and plantar flexion movements in the sagittal plane during gait cycle. The dorsiflexion angle includes [0-12] angles, and the plantar flexion angle includes [0; -15] angles. Trajectory tracking results of the controllers for one gait cycle of is given in Fig. 7. RMS error measurement in angle (°) for gait cycle are presented.

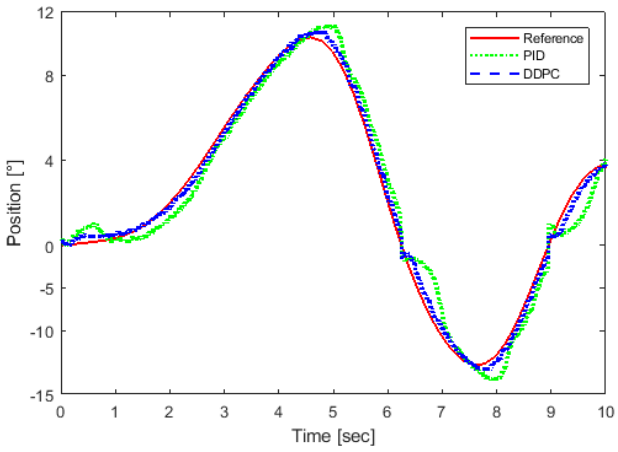

Figure 7. Trajectory tracking performances of the DDPC and PID controller

Examining the RMS error measurements of the trajectory tracking reveals that the DDPC has almost twice the performance of the PID controller. The RMS value for the PID controller is 0.55276°, while this value was calculated as 0.2857° for the data-driven predictive control. The developed P-AFO device outperforms the previous works [39, 40] in trajectory tracking, so it can be understood that the low position tracking error requirement is satisfied.

In the third experiment, stride frequency study was implemented to characterize the tracking performance of the DDPC for several different walking speeds. Trajectory tracking results of the DDPC for varying stride frequencies (0.4 Hz, 0.6 Hz and 0.8 Hz) are presented in Fig. 8. Red lines are the reference signals, while the blue lines represent trajectory tracking results. RMS error measurement in angle (°) for gait cycle are submitted. RMS error measurement in angle (°) for gait cycle are submitted.

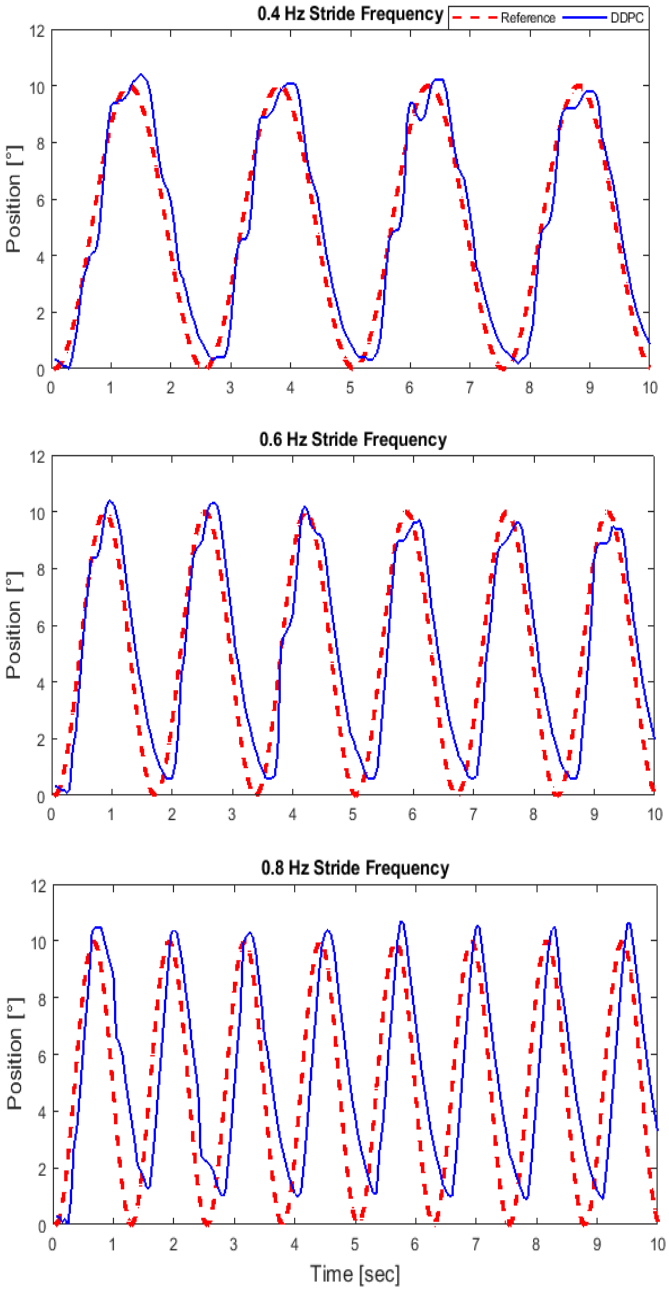

Figure 8. Trajectory tracking performances of the DDPC and PID controller for different stride frequencies

When the tracking results for the multiple stride frequencies shown in Fig. 8 are examined, it can be seen that when the gait cycle frequency is 0.4 Hz, the applied DDPC is much more accurate than it is at higher frequencies. The RMS error value for DDPC algorithm was calculated as 0.4165°, 0.8449°, 1.4457°, respectively for each frequency. At increased walking speed, the tracking error increased with it due to the limited speed of the actuators.

[Downloaded from www.aece.ro on Thursday, July 03, 2025 at 19:18:59 (UTC) by 172.69.6.6. Redistribution subject to AECE license or copyright.]

VI. Conclusion

In this article, we introduced the design and control of a pneumatically powered P-AFO device. The prototype showed the capability of 12° and 20° of dorsiflexion from neutral position and from a plantar flexion position, respectively. The total weight of the developed P-AFO prototype is 2.5 kg excluding the power supply and the air compressor. The prototype also showed repeatability of feed forward control and capability of feedback control for the ankle joint angle.

Experimental studies were performed to compare performances of the controllers. These studies including step and multi-step response, stride frequency, and trajectory tracking were conducted using the P-AFO prototype. Experimental results demonstrate that the overall system satisfied the design requirements and the suggested DDPC is better than a PID controller in trajectory tracking under different conditions.

In future studies, performance comparison of the designed controller with model-based controllers such as impedance, adaptive backstepping etc., could be considered. In addition, different designs will be developed to increase the degree of freedom of the device.

We believe that this data-driven predictive control algorithm, constructed entirely independent of the model, will open a rich space for future rehabilitation techniques for ankle-foot disorders.

References

[1] A. Doğan, M. Mengüllüoğlu, N. Özgirgin, "Evaluation of the effect of ankle-foot orthosis use on balance and mobility in hemiparetic stroke patients," European Journal of Physical and Rehabilitation Medicine, vol. 33, no. 15-16, pp. 1433-1439, 2011. doi:10.3109/09638288.2010.533243

[2] P. R. G. Lucareli, M. D. O. Lima, J. G. D. A. Lucarelli, F. P. S. Lima, "Changes in joint kinematics in children with cerebral palsy while walking with and without a floor reaction ankle-foot orthosis," Clinics, vol. 62, no. 1, pp. 63-68, 2007. doi:10.1590/S1807-59322007000100010

[3] S. J. Korzeniewski, J. Slaughter, M. Lenski, P. Haak, N. Paneth, "The complex aetiology of cerebral palsy," Nature Reviews Neurology, vol. 14, no. 528-543, pp. 528-543, 2018. doi:10.1038/s41582-018-0043-6

[4] A. Cullell, J. C. Moreno, E. Rocon, A. Forner-Cordero, J. L. Pons, "Biologically based design of an actuator system for a knee–ankle–foot orthosis," Mechanism and Machine Theory, vol. 44, no. 4, pp. 860-872, 2009. doi:10.1016/j.mechmachtheory.2008.04.001

[5] M. Nevisipour, C. F. Honeycutt, "The impact of ankle-foot-orthosis (AFO) use on the compensatory stepping response required to avoid a fall during trip-like perturbations in young adults: Implications for AFO prescription and design," Journal of Biomechanics, vol 103,2020, https://doi.org/10.1016/j.jbiomech.2020.109703

[6] L. G. Stansbury, S. J. Lalliss, J. G. Branstetter, M. R. Bagg, J. B. Holcomb, "Amputations in US military personnel in the current conflicts in Afghanistan and Iraq," Journal of Orthopaedic Trauma, vol. 22, no. 1, pp. 43-46, 2008. doi:10.1097/BOT.0b013e31815b35aa

[7] D. J. Weber, R. B. Stein, K. M. Chan, G. Loeb, F. Richmond, R. Rolf, S. L. Chong, "BIONic walk aide for correcting foot drop," IEEE Transactions on Neural Systems and Rehabilitation Engineering, vol. 13, no. 2, pp. 242-246, 2005. doi:10.1109/TNSRE.2005.847385

[8] M. S. Poboroniuc, D. E. Wood, R. Riener, N. N. Donaldson, "A new controller for FES-assisted sitting down in paraplegia," Advances in Electrical and Computer Engineering, vol.10, no.4, pp.9-16, 2010, doi:10.4316/AECE.2010.04002

[9] C. A. Byrne, D. T. O'keeffe, A. E. Donnelly, G. M. Lyons, "Effect of walking speed changes on tibialis anterior EMG during healthy gait for FES envelope design in drop foot correction," Journal of Electromyography and Kinesiology, vol. 17, no. 5, pp. 605-616, 2007. doi:10.1016/j.jelekin.2006.07.008

[10] R. Chin, E. T. Hsiao-Wecksler, E. Loth, G. Kogler, S. D. Manwaring, S. N. Tyson, J. N. Gilmer, "A Pneumatic power harvesting ankle-foot orthosis to prevent foot-drop," Journal of Neuroengineering and Rehabilitation, vol. 6, no. 19, pp. 1-11, 2009. doi:10.1186/1743-0003-6-19

[11] S. Pittaccio, L. Garavaglia, C. Ceriotti, F. Passaretti, "Applications of shape memory alloys for neurology and neuromuscular rehabilitation," Journal of Functional Biomaterials, vol. 6, no. 2, pp. 328-344, 2015. doi:10.3390/jfb6020328

[12] S. Telfer, J. Pallari, J. Munguia, K. Dalgarno, M. McGeough, J. Woodburn, "Embracing additive manufacture: implications for foot and ankle orthosis design," BMC Musculoskeletal Disorders, vol. 13, no. 84, pp. 1-9, 2012. doi:10.1186/1471-2474-13-84

[13] J. A. Blaya, H. Herr, "Adaptive Control of a variable-impedance ankle-foot orthosis to assist drop-foot gait," IEEE Transactions on Neural Systems and Rehabilitation Engineering, vol. 12, no. 1, pp. 24-31, 2004. doi:10.1109/TNSRE.2003.823266

[14] A. W. Boehler, K. W. Hollander, T. G. Sugar, D. Shin, "Design, implementation and test results of a robust control method for a powered ankle foot orthosis (AFO)," IEEE International Conference on Robotics and Automation, pp. 2025-2030, 2008. doi:10.1109/ROBOT.2008.4543504

[15] D. P. Ferris, K. E. Gordon, G. S. Sawicki, A. Peethambaran, "An improved powered ankle–poot orthosis using proportional myoelectric control," Gait & Posture, vol. 23, no. 4, pp. 425-428, 2006. doi:10.1016/j.gaitpost.2005.05.004

[16] D. H. Kuettel III, "Pulley optimization for a walking-engine-actuated active ankle-foot orthosis," Journal of Young Investigators, vol. 31, no. 5, pp. 32-38, 2016. doi:10.22186/jyi.31.5.32-38

[17] Y. Savas, O. Kirtas, H. Bastürk, E. Samur, "A backstepping control design for an active ankle-foot orthosis," IEEE 56th Annual Conference on Decision and Control (CDC), pp. 262-267, 2007. doi:10.1109/CDC.2017.8263676

[18] B. C. Neubauer, J. Nath, W. K. Durfee, "Design of a portable hydraulic ankle-foot orthosis," 36th Annual International Conference of the IEEE Engineering in Medicine and Biology Society, pp. 1182-1185, 2014. doi:10.1109/CDC.2017.8263676

[19] M. Noël, B. Cantin, S. Lambert, C. M. Gosselin, L. J. Bouyer, "An electrohydraulic actuated ankle foot orthosis to generate force fields and to test proprioceptive reflexes during human walking," IEEE Transactions on Neural Systems and Rehabilitation Engineering, vol. 16, no. 4, pp. 390-399, 2008. doi:10.1109/TNSRE.2008.926714

[20] O. Ulkir, G. Akgun, E. Toptas, and E. Kaplanoglu, "Design and myoelectric control of an active orthosis device using finite state machine algorithm", Technium, vol. 2, no. 7, pp. 286–296, Nov. 2020. https://doi.org/10.47577/technium.v2i7.2122

[21] C. M. Thalman, T. Hertzell and H. Lee, "Toward a soft robotic ankle-foot orthosis (SR-AFO) exosuit for human locomotion: preliminary results in late stance plantarflexion assistance," 2020 3rd IEEE International Conference on Soft Robotics (RoboSoft), New Haven, CT, USA, 2020, pp. 801-807, doi:10.1109/RoboSoft48309.2020.9116050

[22] Z. Wang, E. T. Hsiao-Wecksler, "Design of a compact high-torque actuation system for portable powered ankle–foot orthosis," Journal of Medical Devices, vol. 10, no. 3, pp. 1-3, 2016. doi:doi.org/10.1115/1.4033780

[23] R. Jimenez-Fabian, O. Verlinden, "Review of control algorithms for robotic ankle systems in lower-limb orthoses, prostheses, and exoskeletons," Medical Engineering & Physics, vol. 34, no. 4, pp. 397-408, 2012. doi:10.1016/j.medengphy.2011.11.018

[24] M. R. Tucker, J. Olivier, A. Pagel, H. Bleuler, M. Bouri, O. Lambercy, R. Gassert, "Control strategies for active lower extremity prosthetics and orthotics: a review," Journal of Neuroengineering and Rehabilitation, vol. 12, no. 1, pp. 1-29, 2015. doi:10.1186/1743-0003-12-1

[25] A. Agrawal, V. Sangwan, S. K. Banala, S. K. Agrawal, S. A. Binder-Macleod, "Design of a novel two degree-of-freedom ankle-foot orthosis," Journal of Mechanical Design, vol. 129, no. 11, pp. 1137-1143, 2007. doi:10.1115/1.2771231

[26] V. Arnez-Paniagua, H. Rifaï, Y. Amirat, M. Ghedira, J. M. Gracies, S. Mohammed, "Adaptive control of an actuated ankle foot orthosis for paretic patients," Control Engineering Practice, vol. 90, no. 1, pp. 207-220, 2019. doi:10.1016/j.conengprac.2019.06.003

[27] J. F. Guerrero-Castellanos, H. Rifaï, V. Arnez-Paniagua, J. Linares-Flores, L. Saynes-Torres, S. Mohammed, "Robust active disturbance rejection control via control Lyapunov functions: Application to actuated-ankle–foot-orthosis," Control Engineering Practice, vol. 80, no. 2, pp. 49-60, 2018. doi:10.1016/j.conengprac.2018.08.008

[Downloaded from www.aece.ro on Thursday, July 03, 2025 at 19:18:59 (UTC) by 172.69.6.6. Redistribution subject to AECE license or copyright.]

[28] W. Huo, V. Arnez-Paniagua, G. Ding, Y. Amirat, S. Mohammed, "Adaptive proxy-based controller of an active ankle foot orthosis to assist lower limb movements of paretic patients," Robotica, vol. 37, no. 12, pp. 2147-2164, 2019. doi:10.1017/S0263574719000250

[29] Y. Xia, W. Xie, B. Liu, X. Wang, "Data-driven predictive control for networked control systems," Information Sciences, vol. 235, pp. 45-54, 2013. doi:10.1016/j.ins.2012.01.047

[30] O. Ulkir, G. Akgun, E. Kaplanoglu, "Real-time implementation of data-driven predictive controller for an artificial muscle," Studies in Informatics and Control, vol. 28, no. 2, pp. 189-200, 2019. doi:doi.org/10.24846/v28i2y201907

[31] J. Berberich, J. Koehler, M. A. Muller and F. Allgower, "Data-driven model predictive control with stability and robustness guarantees," in IEEE Transactions on Automatic Control, doi:10.1109/TAC.2020.3000182

[32] F. Smarra, A. Jain, T. De Rubeis, D. Ambrosini, A. D'Innocenzo, R. Mangharam, "Data-driven model predictive control using random forests for building energy optimization and climate control," Applied Energy, vol. 226, pp. 1252-1272, 2018. doi:10.1016/j.apenergy.2018.02.126

[33] Z. Hou, S. Liu, T. Tian, "Lazy-learning-based data-driven model-free adaptive predictive control for a class of discrete-time nonlinear systems," IEEE Transactions on Neural Networks and Learning Systems, vol. 28, no. 8, pp. 1914-1928. doi:10.1109/TNNLS.2016.2561702

[34] P. Van Overschee, B. L. De Moor, "Subspace identification for linear systems: theory-implementation-applications," pp. 1-272, Springer Science & Business Media, 2012

[35] R. Kadali, B. Huang, A. Rossiter, "A data driven subspace approach to predictive controller design," Control Engineering Practice, vol. 11, no. 3, pp. 261-278. doi:10.1016/S0967-0661(02)00112-0

[36] A. H. González, A. Ferramosca, G. A. Bustos, J. L. Marchetti, M. Fiacchini, D. Odloak, "Model predictive control suitable for closed-loop re-identification," Systems & Control Letters, vol. 69, pp. 23-33, 2014. doi:10.1016/j.sysconle.2014.03.007

[37] N. Rao, G. Chaudhuri, D. Hasso, K. D'Souza, J. Wening, C. Carlson, A. S. Aruin, "Gait assessment during the initial fitting of an ankle foot orthosis in individuals with stroke," Disability and Rehabilitation: Assistive technology, vol. 3, no. 4, pp. 201-207, 2007. doi:10.1080/17483100801973023

[38] Y. L. Park, B. R. Chen, D. Young, L. Stirling, R. J. Wood, E. Goldfield, R. Nagpal, "Bio-inspired active soft orthotic device for ankle foot pathologies," IEEE/RSJ International Conference on Intelligent Robots and Systems, pp. 4488-4495, 2011. doi:10.1109/IROS.2011.6094933

[39] J. Zhang, Y. Yin, J. Zhu, "Sigmoid-based hysteresis modeling and high-speed tracking control of sma-artificial muscle," Sensors and Actuators A: Physical, vol. 201, pp. 264-273, 2013. doi:10.1016/j.sna.2013.07.036

[40] M. Vivian, M. Reggiani, J. C. Moreno, J. L. Pons, D. Farina, M. Sartori, "A dynamically consistent model of a motorized ankle-foot orthosis," 6th International IEEE/EMBS Conference on Neural Engineering (NER), pp. 1558-1561, 2013. doi:10.1109/NER.2013.6696244